Magnetic Resonance Imaging of Major Histocompatibility Class II Expression in the Renal Medulla Using Immunotargeted Superparamagnetic Iron Oxide Nanoparticles

Kristi L. Hultman,[†] Anthony J. Raffo,[‡] Adrienne L. Grzenda,[§] Paul E. Harris,[‡] Truman R. Brown,[⊥,*] and Stephen O'Brien[†,*]

[†]Department of Applied Physics, Columbia University, 200 SW Mudd Building, New York, New York 10027, [‡]Department of Medicine, Columbia University Medical Center, 630 West 168th Street, New York, New York 10032, [§]Department of Surgery, Columbia University Medical Center, 630 West 168th Street, New York, New York 10032, and [⊥]Department of Radiology, Columbia University, 710 West 168th Street, New York, New York 10032

ABSTRACT We demonstrate the development and successful application of immunotargeted superparamagnetic iron oxide nanoparticles (ITSIONs), with *in vivo* magnetic resonance diagnostic and potential drug delivery capability for kidney disease. Further, the versatility of the conjugation chemistry presents an attractive route to the preparation of a range of biomolecule—nanoparticle conjugates. The ITSION contrast agent is a stable, biocompatible, targeted nanoparticle complex that combines a monodisperse iron oxide nanoparticle core with a functionalized phospholipid coating conjugated to antibodies that is capable of targeting normal cells expressing specific target antigens. The plasma half-life and R1 and R2 relaxivities suggest sufficient time for targeted binding while clearing from the system quick enough for detection of specific contrast enhancement. RT1 anti-MHC Class II antibodies were used to target the renal medulla of the rat, a section of the kidney in which MHC Class II, associated with inflammation, is specifically expressed. For *in vivo* resonance imaging, we compare phospholipid coated nanoparticles, nonspecific ITSIONs, and RT1 ITSIONs. Enhanced binding of the RT1 ITSIONS indicates specificity for the renal medulla and thus potential for disease detection or drug delivery.

KEYWORDS: iron oxide nanoparticles · phospholipid · contrast agents · drug delivery · magnetic resonance imaging · immunotargeted · MHC Class II

The interface between magnetic resonance imaging (MRI) and nanotechnology invites new approaches to the diagnosis and treatment of disease, presenting unique opportunities for contrast agent creation, such as the development of MR-active compounds with target-specific characteristics. The magnetic properties of iron oxide nanoparticles (IONs) are ideally suited for contrast agent creation.[1–4] The challenge in using such particles as targeted MRI contrast agents has been in creating a surface structure that provides sufficient stability under biological conditions, resists nonspecific adsorption, and is easily altered to target a wide range of antigens.[5,6] Immunotargeted superparamagnetic iron oxide nanoparticles (ITSIONs) combine the specificity of antibodies and the contrast behavior of IONs with the *in vivo* lifetime and drug delivery potential of stealth liposomes.[7,8] ITSIONs are monodisperse nanoparticles, comprised of an exterior functionalized phospholipid monolayer surrounding an integrated inorganic iron oxide crystalline core and an organic monolayer of oleic acid alkyl chains. The functional groups in the exterior monolayer can be easily conjugated to a broad range of biological molecules. The phospholipid coating interacts with oleic acid surfactants to create a pseudolipid bilayer surrounding the nanoparticles (possibly similar to a cellular membrane) and renders them highly dispersible in aqueous environments. Due to the nonspecific conjugation method, virtually any protein, peptide, or molecule may be substituted onto the ITSION, allowing for tailor-made molecular MRI contrast agents.[9] Due to their versatility, ITSIONs create possibilities for the molecular diagnosis of disease,[10] cell-level tracking of disease progression,[11,12] tracking of transplanted cells and tissues,[13,14] drug delivery,[15,16] and therapeutics.[16,17] Traditionally, IONs, especially those prepared by aqueous chemistry methods, have exhibited wide size distributions with diameters ranging from 50 nm to >100 nm after coating with a biocompatible substance such as dextran.[18] In this case, we take advantage of the narrow size distributions (made possible by modern decomposition techniques[19]) and

*Address correspondence to trb11@columbia.edu, so188@columbia.edu.

Received for review December 4, 2007 and accepted February 19, 2008.

Published online March 5, 2008.
10.1021/nn700400h CCC: $40.75

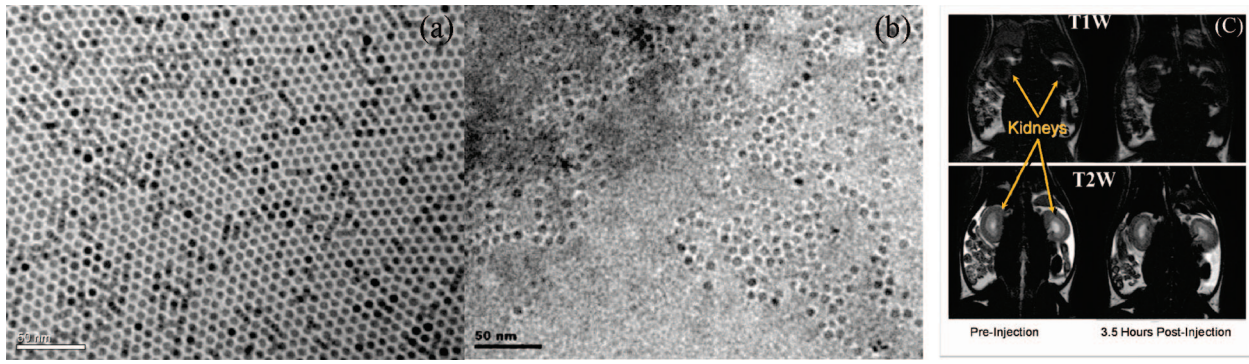

Figure 1. (a) Transmission electron microscopy (TEM) image of uncoated 5 nm γ-Fe_2O_3 nanoparticles evaporated from a hexane solution. The monocrystalline nanoparticles are highly uniform in both size and shape. (b) TEM of mPEG 2000-coated nanoparticles evaporated from phosphate buffer solution and negatively stained with 1% phosphotungstic acid. The coating is visualized as a 2 nm thick white ring surrounding the dark nanoparticles. (c) MR images of Lewis rats injected with unconjugated coated nanoparticles of the kind shown in panel b. The images also serve to show some basic rat anatomy, with both kidneys labeled for T1- and T2-weighted images. No nonspecific binding in the kidney is determined from a return to contrast from $t = 0$ to $t = 3.5$ h.

biocompatibilization of magnetic nanoparticles using phospholipid chemistry[20] in order to extend possibilities for MR contrast agent creation in the 5–20 nm regime. The properties and interactions with biological systems in this unique size regime are of paramount interest in bionanotechnology.

Prior to modification, the nanoparticles have a core diameter of 5 nm (Figure 1a). With a final coated diameter of 10 nm (Figure 1b), the core remains intact and relatively monodisperse ($\sim<$10% deviation with respect to diameter), and the biocompatible product is well defined and therefore suitable for quantitative analysis in MR imaging as demonstrated here. The oleic acid monolayer is believed to be covalently bound to the surface γ-Fe_2O_3,[21] enabling the addition of methoxy-poly(ethylene glycol) (mPEG)-modified phospholipids which create a novel bilayer structure that allows the ITSIONs to evade *in vivo* clearance by the reticuloendothelial system (RES) and extends their plasma lifetime to several hours. A controlled amount of maleimide is present in the outer bilayer for conjugation to antibodies, as well as other proteins, peptides, and molecules. Focusing on these particles, we report here the first recorded observations of immunotargeting of extravascular antigenic sites using magnetic nanoparticles.

A critical issue in the development of *in vivo* immunotargeted agents is their plasma lifetime. If the agent's lifetime is too short, it does not have sufficient opportunity to bind to the target, while if its plasma lifetime is too long, observing sufficient contrast between specifically bound and free compartments becomes difficult. For example, radio-conjugated antibodies have been shown to target specific antigens *in vivo*; however, their lengthy lifetime in the blood often precludes visualization of specific binding.[22] Similarly, a limiting factor in the use of magnetic nanoparticles as immunotargeted contrast agents has been the design and synthesis of an optimal exterior surface of the nanoparticle, allowing it to evade the body's innate immune defense mechanisms while still possessing sufficient flexibility in chemical reactivity. Although a number of coatings now exist—including albumin,[23] dextran,[24,25] pluronic,[15,26] and starch,[27] among others—they are unsatisfactory due to either their instability *in vivo* or their difficulty in being modified to target a range of biological molecules. Moreover, they lack the potential for use in drug delivery due to the nature of the coating.[15,24,28]

As first synthesized, the nanoparticles are strongly hydrophobic due to the oleic acid molecules used as a surfactant in the synthesis. The outer leaflet, or micelle, created by the mPEGylated phospholipids prevents opsinization. Previous studies of stealth liposomes have demonstrated that if the phospholipid density covering the nanoparticles is too low, the polyethylene chain forms a mushroom-like structure.[29,30] Independently, we confirmed that the low-density structure is quickly cleared from the blood in less than 10 min. While there have been several reports of PEG-functionalized nanoparticles used in cell cultures, the complex nature of the *in vivo* environment requires optimization of the coating to minimize interactions and prevent rapid clearance from the vasculature.[31,32] When the density of the phospholipids is increased to 1.5 per nm^2, it is believed that the PEG chains on the phospholipids protrude radially from the core, forming a brush-like structure.[33,34] Because the PEGylated phospholipids interact with the oleic acid surfactants in a manner similar to phospholipids in a cellular membrane, we believe this should provide more flexibility in the interactions with cellular membranes due to the fluidity of the phospholipid coating. These structures hinder plasma proteins from attaching to the surface and significantly delay removal by the liver's RES cells. In addition, it is possible to conceive the notion of "tuning" the plasma lifetime of the ITSION as a function of mPEG size or chain length. We postulate that a brush-like structure exists for the ITSION coated with predominantly mPEG 2000 phospholipids, as depicted in Figure 2.

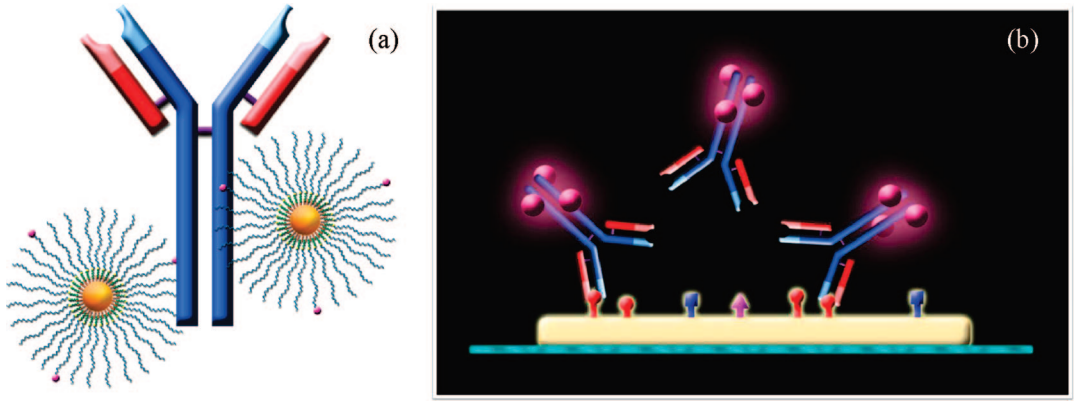

Figure 2. (a) Schematic depicting the construction of the immunotargeted superparamagnetic iron oxide nanoparticle (ITSION). The iron oxide core (yellow, not to scale) is encapsulated in a brush-like shell of mPEG phospholipids. Maleimide-functionalized mPEG phospholipids can bind to the antibody after modification to create R-SH groups, using Traut's reagent. (b) Schematic depicting specific binding of the antibody to antigens on the tissue surface.

The optimal bilayer structure for coating the nanoparticles for use as contrast agents is a uniform 2 nm thick shell of phospholipids with no aggregation (Figure 1b). When coated with lower amounts of phospholipids, the nanoparticles tend to settle out of solution and are rapidly cleared from the blood, as determined by FACS analysis (see Supporting Information). Different lengths of mPEG phospholipids can also be used; however, PEG chains shorter than 750, even at maximum concentrations, were incapable of preventing aggregation. Previous research indicates that mPEG 2000 and mPEG 5000 are better at resisting nonspecific binding of proteins *in vivo* and have longer circulation times than their shorter counterparts.[33–36] In view of this, mPEG 2000 was thought to be optimal. In order to provide binding sites for conjugation, 2% mPEG 2000: maleimide was added to the mPEG 2000 phospholipids, resulting in nanoparticles that can be conjugated to a wide range of compounds. To aid *in vitro* detection, 2% rhodamine or fluorescein-tagged phospholipids (Avanti) were also added.

The spin–lattice (R1) and spin–spin (R2) relaxivities were measured in 1% agarose phantoms of the coated γ-Fe_2O_3 nanoparticles using a 3 T Philips Achieva scanner. For T1-weighted scans, the nanoparticles behave as positive contrast agents for concentrations below 500 nM (Figure 3a). At concentrations of 500 nM and above, the T2 effects overpower the T1 effects. The use of manganese oxide nanoparticles has been proposed in order to circumvent this issue. Addtionally, the sweep imaging with Fourier transformation (SWIFT) sequence under development by the Garwood group shows great potential for imaging materials with rapid transverse relaxation rates, allowing for high-resolution images that are highly sensitive to the ITSIONS.[37,38] The nanoparticles behave as negative contrast agents for T2-weighted scan sequences, with a significant decrease in the image intensity for concentrations around 10 nM (Figure 3b). Quantitatively, at 3 T, the R1 relaxivity is 25.8 $\mu M^{-1}\ s^{-1}$ and the R2 relaxivity is 266 $\mu M^{-1}\ s^{-1}$ for 6 nm γ-Fe_2O_3 nanoparticles. These are considerably higher than the values reported at 3 T by Cheon for similar sized MnO nanoparticles, R1 = 3 $\mu M^{-1}\ s^{-1}$ and R2 = 14 $\mu M^{-1}\ s^{-1}$,[8] and for ferumoxtran-10, R1 = 6.58 $mM^{-1}\ s^{-1}$ and R2 = 127.8 $mM^{-1}\ s^{-1}$.[39]

In choosing an antibody to conjugate to the nanoparticles, the first consideration is to use one with sufficient antigen binding sites on an easily imaged organ. Taking 10 nM as the detection limit, a cell of volume 10^4 μm^3 requires 6×10^4 binding sites for observation. We chose to target ITSIONs toward Major Histocompatibility Class II (MHC II) molecules, a transmembrane, tissue-restricted macromolecular marker of adaptive immune responses and inflammation, using RT1 antibodies specific for rat MHC II molecules.[40,41] Previous attempts to image inflammation using iron oxide nanoparticles have been dependent on nonspecific uptake by macrophages which accumulate at sites of inflammation.[12,42,43] In both human and rat, MHC II molecules are constitutively expressed in the medulla of the kidney, albeit in slightly different microanatomical regions.[44,45] The cell surface density of MHC II molecules in rodent cells has been estimated (using radioiodinated anti-MHC II antibodies) to be on the order of 10^4-10^6 per cell,[46–49] in the range we can expect to detect.

RT1 anti-MHC II antibodies are conjugated to the maleimide-functionalized mPEG 2000 phospholipid coating by a simple two-step procedure. First, the antibodies are modified using Traut's reagent to transform a fraction of the antibody's primary amine groups into thiols. Next, the modified antibody is mixed with the nanoparticles, forming a thioether linkage between them (see Supporting Information). On the basis of iron and protein concentration measurements, there are two nanoparticles per antibody on average. We immunostained nearby sections of paraffin-embedded rat kidney with the rhodamine-tagged ITSIONs (Figure 4b) and unconjugated RT1 antibodies to serve as controls

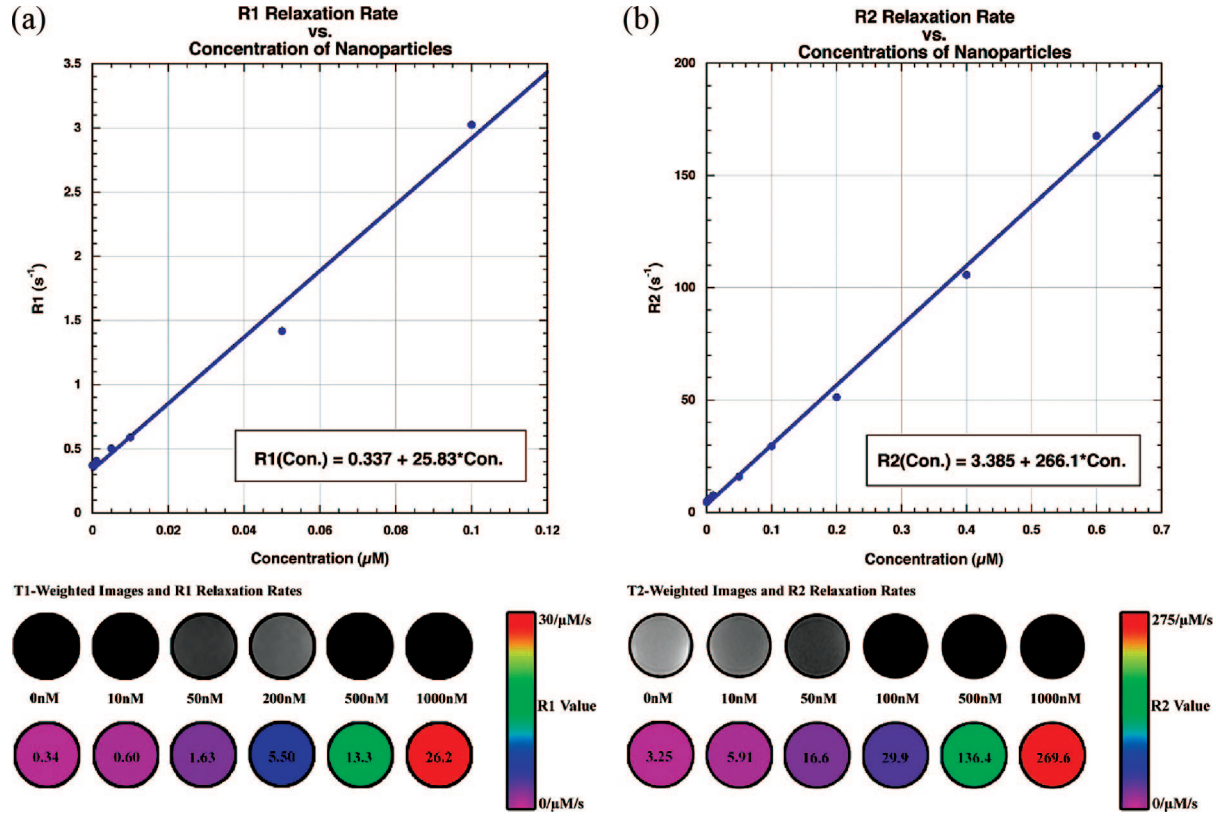

Figure 3. T1 and T2 relaxivity measurements. Iron oxide phantoms in 1% agarose gel. (a) T1-weighted spin–echo MR images and R1 color map for nanoparticle concentrations from 10 to 1000 nM, scanned at 3 T. The R1 relaxivity increases linearly with concentration at a rate of 25.83 μM^{-1} s^{-1}. While the contrast increases with concentration, above 200 nM, the contrast decreases as the T2 effects begin to overtake the T1 effects. (b) T2-weighted TSE MR images and R2 color maps. The R2 relaxivity increases linearly with concentration at a rate of 266.1 μM^{-1} s^{-1}. At concentrations above 500 nM, the signal is difficult to distinguish from the background.

(Figure 4a) to confirm the conjugation and the continued selectivity of the RT1 antibody−nanoparticle pair.

MHC II is localized primarily to the renal medulla with minimal expression in the renal cortex or pelvis. Comparison between panels a and b of Figure 4 shows the same binding pattern, indicating that antibody function remains undisturbed due to the conjugation.

To test the RT1 ITSIONs *in vivo*, 200 μL aliquots of a 100 μM solution of RT1 ITSIONs were injected intravenously into rats. We found no signs of toxicity (weight loss, abnormal behavior, reproductive capacity) in rats used in these studies. At least five rats received multiple injections of conjugate (>4 times) over 4 months. Control injections consisted of unconjugated coated nanoparticles and ITSIONs conjugated to goat anti-guinea pig antibodies, which are nonspecific in the rat. The effects on the contrast in the rat kidney were followed by T2-weighted MRI prior to injection and for 2 h subsequently (Figure 5). As shown in the left column of Figure 5, all three

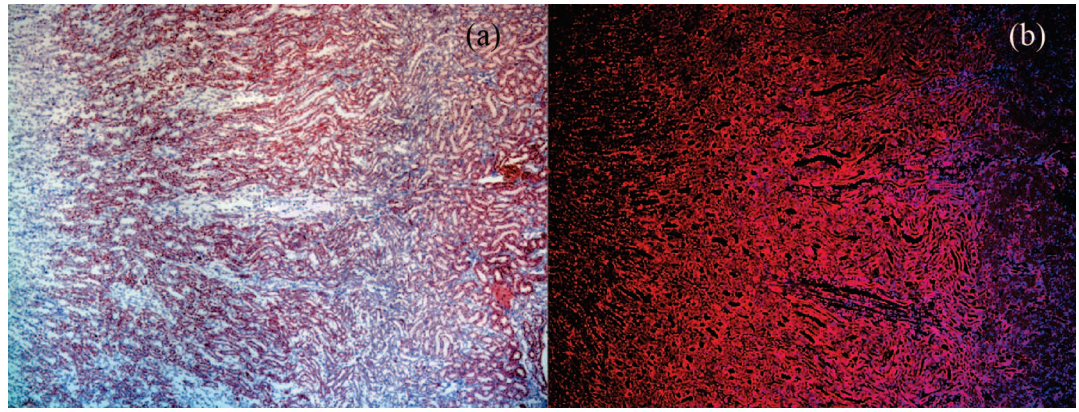

Figure 4. RT1 expression in the rat kidney. (a) Rat kidney immunostained using RT1 anti-MHC II antibodies. MHC II is expressed in the inner and outer zones of the proximal renal tubules, as well as the medullary capillary plexus. (b) Rat kidney immunostained using rhodamine-tagged RT1 ITSIONs. The staining pattern is identical, indicating successful conjugation of the antibodies to the nanoparticles without disruption of antibody avidity.

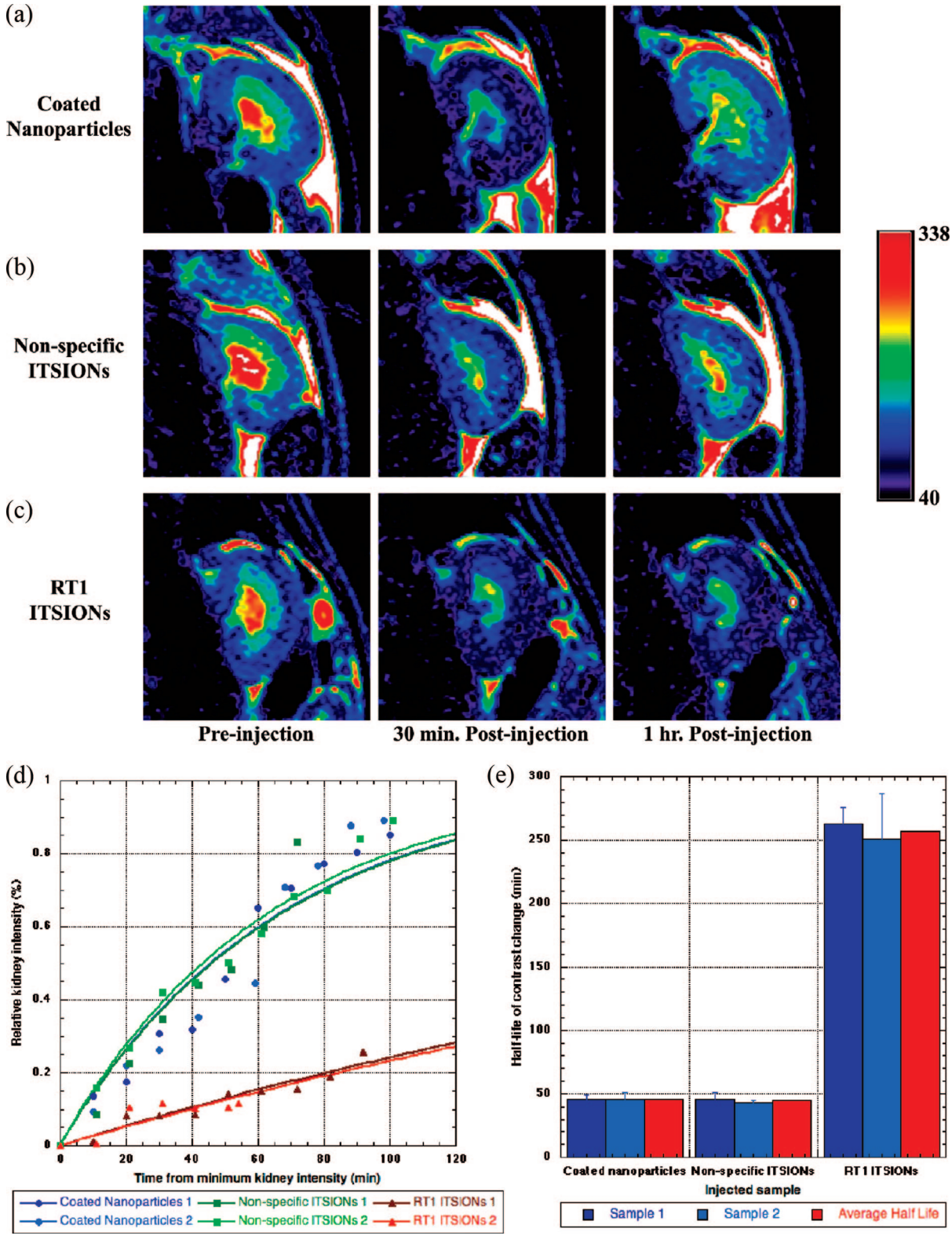

Figure 5. ITSION targeting of MHC II-expressing cells in the kidney. T2-weighted turbo spin–echo MRI of rat kidneys pre-injection and at 30 min, 1 h, and 2 h post-injection with (a) unconjugated nanoparticles, (b) nonspecific ITSIONs, and (c) RT1 ITSIONs. The images have been color-mapped by intensity. (d) Change in the relative contrast intensity of the rat kidney pre- and post-injection for unconjugated and RT1 ITSIONs. (e) The unconjugated nanoparticles have a half-life of 45 min in the bloodstream, while the RT1 ITSIONs have a half-life of 255 min.

regions of the kidney, cortex, medulla, and pelvis are visible prior to the injection.

In all cases, the contrast between the medulla and the cortex is significantly reduced following injection, reaching a minimum 30 min post-injection. The change in contrast is strongest and lasts the longest in the case of the RT1 ITSIONs. In this case, the R2 value increases from 13 to 22 s^{-1} in the medulla, and there is minimal visualization of the medulla at 2 h. For the unconjugated coated nanoparticles and goat anti-guinea pig ITIONS (nonspecific ITSIONs hereafter), the contrast returns to the initial intensity level within 2 h, as shown by the right column in Figure 5a−c.

Figure 5d shows the change in the signal intensity from the medulla normalized to the change at 30 min over time. Unconjugated coated nanoparticles and nonspecific ITSIONs both have an elimination half-life of 45 min in the kidney (Figure 5e). However, RT1 ITSIONs have a half-life of 255 min, a 500% increase over that of the unconjugated coated nanoparticles, indicating the specific binding of the conjugate nanoparticles to the MHC II antigens in the renal medulla. In terms of effects on the antibody alone, we speculate that conjugation would only reduce avidity of the antibody (see Supporting Information).

We can estimate the concentration of binding sites in the medulla from the R2 change (9 s^{-1}) using our measured relaxivity of 266 μM^{-1} s^{-1}. This corresponds to a concentration of 34 nM, or 2×10^5 sites per cell for a typical cell of volume 10^4 μm^3.

CONCLUSIONS

Using phospholipid coatings, magnetic nanoparticles can be synthesized with extended plasma lifetimes. Inclusion of maleimide in the phospholipid coating allows the particles to be conjugated to a wide range of compounds, antibodies in particular. The resulting particle, which we have termed an ITSION, is a selective immunotargeted agent with novel binding characteristics suitable for detailed pharmacokinetic analysis and quantization of target densities, as we have shown by their time-course-specific effects on MRI contrast in the rat kidney. At 3 T, the ITSIONs have an R1 relaxivity of 25.8 μM^{-1} s^{-1} and an R2 relaxivity of 266 μM^{-1} s^{-1} for the 6 nm phospholipid-coated γ-Fe_2O_3 nanoparticles. The ITSIONs have a plasma half-life of 45 ± 5 min, providing sufficient time for targeted binding while clearing from the system quickly enough for easy detection of specific contrast enhancement. The functionalized phospholipid coating allows for effective high-yield conjugation to virtually any protein or antibody. For these experiments, RT1 anti-MHC II antibodies were used to target the renal medulla of the rat. While the contrast in the kidneys returns to its original intensity within 2 h for rats injected with nonspecific ITSIONs, in rats injected with the RT1 ITSIONs the contrast remains much longer, with a relaxivity change of 9 s^{-1}, corresponding to a ITSION concentration of 34 nM in the kidneys.

METHODS

Materials. Iron pentacarbonyl ($Fe(CO)_5$), technical grade oleic acid (OA), trioctylamine (TOA), and trimethylamine-*N*-oxide were purchased from Sigma Aldrich (St. Louis, MO). 1,2-Distearoyl-*sn*-glycero-3-phosphoethanolamine-*N*-[methoxy-poly(ethylene glycol)-2000] (mPEG 2000), 1,2-distearoyl-*sn*-glycero-3-phosphoethanolamine-*N*-[maleimide-poly(ethylene glycol)-2000] (maleimide-mPEG 2000), 1,2-dioleoyl-*sn*-glycero-3-phosphoethanolamine-*N*-(carboxyfluorescein) (green phospholipid), and 1,2-dioleoyl-*sn*-glycero-3-phosphoethanolamine-*N*-(Lissamine Rhodamine B Sulfonyl) (red phospholipid) were purchased from Avanti Polar Lipids (Alabaster, AL). Traut's reagent (2-iminothiolane · HCl) was purchased from Pierce Biotechnology (Rockford, IL). RT1 mouse anti-MHC II antibodies were purchased from Cedarlane (Ontario, Canada).

Nanoparticle Synthesis and Characterization. The γ-Fe_2O_3 nanoparticles were synthesized using a procedure slightly modified from the Hyeon method.[19] First, 3.04 mmol of $Fe(CO)_5$ was injected rapidly into a preheated solution of 9.45 mmol of OA (3 mL) and 34.31 mmol of TOA (15 mL), and then the solution was heated to reflux until nucleation of FeO_x nanoparticles occurred. Ten minutes post-nucleation, the solution was cooled below 130 °C, and 9.32 mmol of dehydrated trimethylamine-*N*-oxide (0.7 g) was added. The solution was then heated to 130 °C for 2 h, followed by heating to reflux for 1 h. Finally, the solution was cooled and washed with ethanol and hexane. The nanoparticle samples were characterized by transmission electron microscopy (TEM, Joel CX100) with an accelerating voltage of 100 kV. A single drop of dilute solution of nanoparticles in hexane was placed on a 400 mesh copper grid with Formvar backing. Samples were vaccuum-dried for at least 1 h prior to imaging.

Phospholipid Coating and Characterization. The nanoparticles were coated with phospholipids using a technique similar to the Dubertret method.[28] A 400 μL sample of nanoparticles was precipitated with methanol and centrifuged. Following removal of the supernatant, the precipitated nanoparticles were dried in a vacuum. Next, phospholipids in a 96:2:2 molar ratio of mPEG 2000:maleimide-mPEG 2000:rhodamine or fluorescein-conjugated phospholipids were dispersed in chloroform and added to the dried nanoparticles. Chloroform was evaporated from the solution, and phosphate buffer solution (PBS) was added prior to centrifugation, which removed precipitate and excess phospholipids. Finally, the coated nanoparticles were redispersed in PBS at a concentration of 10 mg/mL. The phospholipid coating on the nanoparticles was visualized *via* TEM by placing one drop of a 1% phosphotungstic acid stain on a prepared nanoparticle grid and allowing the water to evaporate for at least 12 h prior to imaging. The concentration of the coated nanoparticle solution and density of the phospholipid coating were determined by UV/vis spectroscopy.

Nanoparticle−Antibody Conjugation. Antibodies were modified for conjugation using Traut's reagent according to the manufacturer's instructions (Pierce). The antibody solution was then mixed with maleimide-functionalized phospholipid-coated nanoparticles at a ratio of two nanoparticles per antibody and allowed to react overnight at 4 °C. For optimal conjugation results, conjugation to the antibodies was always completed immediately following the coating process, as the maleimide functional groups hydrolyze in several hours and lose their reactivity. The nanoparticles were centrifuged to remove unconjugated antibodies and concentrated to a final nanoparticle concentration of 10 mg/mL (50 μM). The concentration of the

antibodies in the solution was measured *via* standard BCA assay (Pierce).

Immunohistochemistry. Five micrometer, sagittal paraffin-embedded rat kidney sections were deparaffinized and rehydrated with xylenes and graded ethanols, respectively. Antigen retrieval was achieved by trypsin digestion for 20 min. Endogenous peroxidase was blocked with a 3% hydrogen peroxide solution for 20 min. Nonspecific binding was blocked with CAS Block (Zymed) for 1 h. Sections were incubated overnight with rhomadine-tagged RT1 ITSIONs (1:50) at 4 °C and counterstained with Hoechst solution (Sigma). Control sections were incubated overnight with RT1 anti-MHC II antibody (1:50) at 4 °C. Biotinylated goat anti-mouse IgG secondary (Vector) followed by HRP-strepavidin (Zymed) and a Nova Red substrate (Vector) were used to visualize the reaction product. Sections were counterstained using hematoxylin (Vector). All microscopy and imaging were done on a Nikon Eclipse E600 apparatus (×4 objective, Nikon Inc., Melville, NY) with Spot RT Slider digital camera and software (Diagnostic Instruments, Sterling Heights, MI).

Flow Cytometry. The lifetime of fluorescein-tagged unconjugated coated nanoparticles and ITSIONs in the blood was measured *via* flow cytometry. Male Lewis rats (Harlan Sprague–Dawley, Inc.) were injected with a dose of 6 mg/kg (200 μL for a 300 g rat). Blood samples were taken from the tail vein pre-injection and at 15, 30, 45, 60, 90, 120, and 150 min intervals post-injection. The blood was diluted at a ratio of 1:60 with 5 mM EDTA−PBS solution, and the fluorescence measured *via* FACS analysis.

MRI Experiments. All MRI experiments were performed using a 3 T Philips Acheiva MRI scanner with a Flex-M coil. The R1 value was measured using a series of inversion–recovery scans with the following settings: TR = 5500 ms, TE = 144 ms, TSE = 34, and inversion–recovery times ranging from 300 to 2500 ms, in 100 ms increments. For T1-weighted MR images, a multi-slice, spin–echo sequence was used with the following scan parameters: TE = 15 ms, TR = 500 ms, flip angle = 60°, NSA = 2 with a voxel size of 0.5 mm × 0.6 mm and a slice thickness of 1.5 mm. The R2 value was measured using a Carr−Purcell−Meiboom−Gill (CPMG) sequence using the following settings: TR = 2000 ms, 20 echos with 20 ms echo spacing, NSA = 1, 1 mm slice thickness, and 0.65 mm × 0.82 mm resolution. For T2-weighted images, a multi-slice turbo spin–echo sequence with a TSE factor of 19 was used with the following parameters: TE = 100 ms, TR = 5000 ms, flip angle = 90°, NSA = 4 with a voxel size of 0.5 mm × 0.6 mm and a slice thickness of 1.5 mm. For animal scans, male Lewis rats (Harlan Sprague–Dawley, Inc.) were sedated and injected with a dose of 6 mg/kg (200 μL for a 300 g rat). To measure the half-life of the nanoparticles in the kidney, T1W and T2W MR images of the rat kidney were taken pre-injection and at 10 min intervals post-injection for 3 h. Images were analyzed using OsiriX (Netfirms). To compare contrast change, regions of interest were drawn around the renal cortex and medulla and the intensities measured. The 30 min mark, where the largest contrast change is evident, was selected as the minimum intensity factor. Prior to normalization, this minimum factor was subtracted from all intensity measurements to account for variations between rats. While the change in the medulla exceeded that of the cortex, their half-life properties were identical, and, as such, the intensity changes were an average of the two regions.

Acknowledgment. This work was supported by PHS, NIH, NIDDK, 2 RO1 DK63567-03, 5P01CA041078-14 (T.R.B.), and the Columbia University DERC (5 P30 DK063608-02). S.O. is grateful for support for this project from CAREER Award No. DMR-0348938. S.O. and K.H. thank A. L. Willis and N. J. Turro for useful discussions at the early stages of this project.

Supporting Information Available: Conjugation schematic, immunohistochemistry, flow cytometry data, and further MRI images and kidney intensity data. This material is available free of charge *via* the Internet at http://pubs.acs.org.

REFERENCES AND NOTES

1. Bulte, J. W.; Douglas, T.; Mann, S.; Frankel, R. B.; Moskowitz, B. M.; Brooks, R. A.; Baumgarner, C. D.; Vymazal, J.; Strub, M. P.; Frank, J. A. Magnetoferritin: Characterization of a Novel Superparamagnetic MR Contrast Agent. *J. Magn. Reson. Imaging* **1994**, *4*, 497–505.
2. Weissleder, R.; Cheng, H. C.; Bogdanova, A.; Bogdanov, A. Magnetically Labeled Cells Can Be Detected by MR Imaging. *J. Magn. Reson. Imaging* **1997**, *7*, 258–263.
3. Weissleder, R.; Elizondo, G.; Wittenberg, J.; Rabito, C. A.; Bengele, H. H.; Josephson, L. Ultrasmall Superparamagnetic Iron Oxide: Characterization of a New Class of Contrast Agents for MR Imaging. *Radiology* **1990**, *175*, 489–493.
4. Yeh, T. C.; Zhang, W.; Ildstad, S. T.; Ho, C. Intracellular Labeling of T-Cells with Superparamagnetic Contrast Agents. *Magn. Reson. Med.* **1993**, *30*, 617–625.
5. Denizot, B.; Tanguy, G.; Hindre, F.; Rump, E.; Jacques Le Jeune, J.; Jallet, P. Phosphorylcholine Coating of Iron Oxide Nanoparticles. *J. Colloid Interface Sci.* **1999**, *209*, 66–71.
6. Zhang, Y.; Dodd, S. J.; Hendrich, K. S.; Williams, M.; Ho, C. Magnetic Resonance Imaging Detection of Rat Renal Transplant Rejection by Monitoring Macrophage Infiltration. *Kidney Int.* **2000**, *58*, 1300–1310.
7. Drummond, D. C.; Meyer, O.; Hong, K.; Kirpotin, D. B.; Papahadjopoulos, D. Optimizing Liposomes for Delivery of Chemotherapeutic Agents to Solid Tumors. *Pharmacol. Rev.* **1999**, *51*, 691–743.
8. Lee, J. H.; Huh, Y. M.; Jun, Y. W.; Seo, J. W.; Jang, J. T.; Song, H. T.; Kim, S.; Cho, E. J.; Yoon, H. G.; Suh, J. S. Artificially Engineered Magnetic Nanoparticles for Ultra-Sensitive Molecular Imaging. *Nature Med.* **2007**, *13*, 95–99.
9. Hultman, K.; Willis, A.; O'Brien, S.; Brown, T. R.; Harris, P.; Turro, N. J.; Grzenda, A. L. Synthesis and Conjugation of Iron Oxide Nanoparticles to Antibodies for Targeting Specific Cells Using Fluorescence and MR Imaging Techniques. U.S. Patent Appl. 20070059775, March 29, 2006.
10. Weissleder, R.; Elizondo, G.; Wittenberg, J.; Lee, A. S.; Josephson, L.; Brady, T. J. Ultrasmall Superparamagnetic Iron Oxide: An Intravenous Contrast Agent for Assessing Lymph Nodes with MR Imaging. *Radiology* **1990**, *175*, 494–498.
11. Isobe, M.; Narula, J.; Southern, J. F.; Strauss, H. W.; Khaw, B. A.; Haber, E. Imaging the Rejecting Heart. In Vivo Detection of Major Histocompatibility Complex Class II Antigen Induction. *Circulation* **1992**, *85*, 738–746.
12. Wu, Y. L.; Ye, Q.; Foley, L. M.; Hitchens, T. K.; Sato, K.; Williams, J. B.; Ho, C. In Situ Labeling of Immune Cells with Iron Oxide Particles: An Approach to Detect Organ Rejection by Cellular MRI. *Proc. Natl. Acad. Sci.* **2006**, *103*, 1852–1857.
13. Corot, C.; Robert, P.; Idee, J. M.; Port, M. Recent Advances in Iron Oxide Nanocrystal Technology for Medical Imaging. *Adv. Drug Delivery Rev.* **2006**, *58*, 1471–1504.
14. Jendelova, P.; Herynek, V.; Urdzikova, L.; Glogarova, K.; Kroupova, J.; Andersson, B.; Bryja, V.; Burian, M.; Hajek, M.; Sykova, E. Magnetic Resonance Tracking of Transplanted Bone Marrow and Embryonic Stem Cells Labeled by Iron Oxide Nanoparticles in Rat Brain and Spinal Cord. *J. Neurosci. Res.* **2004**, *76*, 232–243.
15. Jain, T. K.; Morales, M. A.; Sahoo, S. K.; Leslie-Pelecky, D. L.; Labhasetwar, V. Iron Oxide Nanoparticles for Sustained Delivery of Anticancer Agents. *Mol. Pharmaceutics* **2005**, *2*, 194–205.
16. Ito, A.; Kuga, Y.; Honda, H.; Kikkawa, H.; Horiuchi, A.; Watanabe, Y.; Kobayashi, T. Magnetite Nanoparticle-Loaded Anti-Her2 Immunoliposomes for Combination of Antibody Therapy with Hyperthermia. *Cancer Lett.* **2004**, *212*, 167–175.
17. Simberg, D.; Duza, T.; Park, J. H.; Essler, M.; Pilch, J.; Zhang, L.; Derfus, A. M.; Yang, M.; Hoffman, R. M.; Bhatia, S. Biomimetic Amplification of Nanoparticle Homing to Tumors. *Proc. Natl. Acad. Sci.* **2007**, *104*, 932–936.

18. Stark, D. D.; Weissleder, R.; Elizondo, G.; Hahn, P. F.; Saini, S.; Todd, L. E.; Wittenberg, J.; Ferrucci, J. T. Superparamagnetic Iron Oxide: Clinical Application as a Contrast Agent for MR Imaging of the Liver. *Radiology* **1988**, *168*, 297–301.
19. Hyeon, T.; Lee, S. S.; Park, J.; Chung, Y.; Na, H. B. Synthesis of Highly Crystalline and Monodisperse Maghemite Nanocrystallites without a Size-Selection Process. *J. Am. Chem. Soc.* **2001**, *123*, 12798–12801.
20. Grancharov, S.; Zeng, H.; Sun, S.; Wang, S. X.; O'Brien, S. P.; Murray, C. B.; Kirtley, J. R.; Held, G. A. Bio-Functionalization of Monodisperse Magnetic Nanoparticles and Their Use as Biomolecular Labels in a Magnetic Tunnel Junction Based Sensor. *J. Phys. Chem. B* **2005**, *109*, 13030–13035.
21. Willis, A. L.; Turro, N. J.; O'Brien, S. Spectroscopic Characterization of the Surface of Iron Oxide Nanocrystals. *Chem. Mater.* **2005**, *17*, 5970–5975.
22. Goldenberg, D. M.; Sharkey, R. M.; Paganelli, G.; Barbet, J.; Chatal, J. F. Antibody Pretargeting Advances Cancer Radioimmunodetection and Radioimmunotherapy. *J. Clin. Oncol.* **2006**, *24*, 823–834.
23. Renshaw, P. F.; Owen, C. S.; McLaughlin, A. C.; Frey, T. G.; Leigh, J. S. Ferromagnetic Contrast Agents: A New Approach. *Magn. Reson. Med.* **1986**, *3*, 217–225.
24. Reimer, P.; Jahnke, N.; Fiebich, M.; Schima, W.; Deckers, F.; Marx, C.; Holzknecht, N.; Saini, S. Hepatic Lesion Detection and Characterization: Value of Nonenhanced MR Imaging, Superparamagnetic Iron Oxide-Enhanced MR Imaging, and Spiral Ct-Roc Analysis. *Radiology* **2000**, *217*, 152–158.
25. Zhao, M.; Kircher, M. F.; Josephson, L.; Weissleder, R. Differential Conjugation of Tat Peptide to Superparamagnetic Nanoparticles and Its Effect on Cellular Uptake. *Bioconjugate Chem.* **2002**, *13*, 840–844.
26. Thunemann, A. F.; Schutt, D.; Kaufner, L.; Pison, U.; Mohwald, H. Maghemite Nanoparticles Protectively Coated with poly(ethylene imine) and poly(ethylene oxide)-*block*-poly(glutamic acid). *Langmuir* **2006**, *22*, 2351–2357.
27. Veiga, V.; Ryan, D. H.; Sourty, E.; Llanes, F. Machessault Formation and Characterization of Superparamagnetic Crosslinked High-Amylose Starch. *Carbohydr. Polym.* **2000**, *42*, 353–357.
28. Dubertret, B.; Skourides, P.; Norris, D. J.; Noireaux, V.; Brivanlou, A. H.; Libchaber, A. In Vivo Imaging of Quantum Dots Encapsulated in Phospholipid Micelles. *Science* **2002**, *298*, 1759–1762.
29. Senior, J.; Delgado, C.; Fisher, D.; Tilcock, C.; Gregoriadis, G. Influence of Surface Hydrophilicity of Liposomes on Their Interaction with Plasma Protein and Clearance from the Circulation: Studies with Poly(Ethylene Glycol)-Coated Vesicles. *Biochim. Biophys. Acta* **1991**, *1062*, 77–82.
30. Klibanov, A. L.; Maruyama, K.; Torchilin, V. P.; Huang, L. Amphipathic Polyethyleneglycols Effectively Prolong the Circulation Time of Liposomes. *FEBS Lett.* **1990**, *268*, 235–237.
31. Veiseh, O.; Sun, C.; Gunn, J.; Kohler, N.; Gabikian, P.; Lee, D.; Bhattarai, N.; Ellenbogen, R.; Sze, R.; Hallahan, A. Optical and MRI Multifunctional Nanoprobe for Targeting Gliomas. *Nano Lett.* **2005**, *5*, 1003–1008.
32. Williams, D. N.; Ehrman, S. H.; Holoman, T. R. P. Evaluation of the Microbial Growth Response to Inorganic Nanoparticles. *J. Nanobiotechnol.* **2006**, *4*, 3.
33. Moghimi, S. M.; Hunter, A. C.; Murray, J. C. Long-Circulating and Target-Specific Nanoparticles: Theory to Practice. *Pharmacol. Rev.* **2001**, *53*, 283–318.
34. Moghimi, S. M.; Szebeni, J. Stealth Liposomes and Long Circulating Nanoparticles: Critical Issues in Pharmacokinetics, Opsonization and Protein-Binding Properties. *Prog. Lipid Res.* **2003**, *42*, 463–478.
35. Allen, T. M.; Hansen, C.; Martin, F.; Redemann, C.; Yau-Young, A. Liposomes Containing Synthetic Lipid Derivatives of Poly(Ethylene Glycol) Show Prolonged Circulation Half-Lives in Vivo. *Biochim. Biophys. Acta* **1991**, *1066*, 29–36.
36. Moghimi, S. M. The Effect of Methoxy-Peg Chain Length and Molecular Architecture on Lymph Node Targeting of Immuno-PEG Liposomes. *Biomaterials* **2006**, *27*, 136–144.
37. Na, H. B.; Lee, J. H.; An, K.; Park, Y. I.; Park, M.; Lee, I. S.; Nam, D. H.; Kim, S. T.; Kim, S. H.; Kim, S. W. Development of a T1 Contrast Agent for Magnetic Resonance Imaging Using MNO Nanoparticles. *Angew. Chem., Int. Ed.* **2007**, *46*, 5397–5401.
38. Idiyatullin, D.; Corum, C.; Park, J. Y.; Garwood, M. Fast and Quiet MRI Using a Swept Radiofrequency. *J. Magn. Reson.* **2006**, *181*, 342–349.
39. Simon, G. H.; Bauer, J.; Saborovski, O.; Fu, Y.; Corot, C.; Wendland, M. F.; Daldrup-Link, H. E. T1 and T2 Relaxivity of Intracellular and Extracellular Uspio at 1.5t and 3t Clinical MR Scanning. *Eur. Radiol.* **2006**, *16*, 738–745.
40. Paul, L. C.; Paradysz, J. M.; Milford, E. L.; Kunz, H. W.; Carpenter, C. B. Expression of Rt1.A and Rt1.B/D Antigens on Endothelium of Rat Kidneys. *Transplantation* **1982**, *34*, 121–128.
41. Roos, A.; Schilder-Tol, E. J.; Chand, M. A.; Weening, J. J.; Aten, J. Hgcl2 and Il4 Differentially Modify Expression of Major Histocompatibility Complex Class II Molecules Rt1.B and Rt1.D in B Lymphocytes from Brown Norway and Lewis Rats. *Transplantation Proc.* **1997**, *29*, 1675–1676.
42. Beckmann, N.; Falk, R.; Zurbrugg, S.; Dawson, J.; Engelhardt, P. Macrophage Infiltration into the Rat Knee Detected by MRI in a Model of Antigen-Induced Arthritis. *Magn. Reson. Med.* **2003**, *49*, 1047–1055.
43. Trivedi, R. A.; Mallawarachi, C.; JM, U. K.-I.; Graves, M. J.; Horsley, J.; Goddard, M. J.; Brown, A.; Wang, L.; Kirkpatrick, P. J.; Brown, J.; *et al.* Identifying Inflamed Carotid Plaques Using in Vivo Uspio-Enhanced Mr Imaging to Label Plaque Macrophages. *Arterioscler. Thromb. Vasc. Biol* **2006**, *26*, 1601–1606.
44. Muczynski, K. A.; Ekle, D. M.; Coder, D. M.; Anderson, S. K. Normal Human Kidney Hla-Dr-Expressing Renal Microvascular Endothelial Cells: Characterization, Isolation, and Regulation of MHC Class II Expression. *J. Am. Soc. Nephrol.* **2003**, *14*, 1336–1348.
45. Metzger, R.; Mempel, T.; Joppich, I.; Till, H. Organ-Specific Distribution of Major Histocompatibility Antigens in Rats. *Pediatr. Surg. Int.* **2000**, *16*, 285–292.
46. Lavoie, P. M.; McGrath, H.; Shoukry, N. H.; Cazenave, P. A.; Sekaly, R. P.; Thibodeau, J. Quantitative Relationship between MHC Class II-Superantigen Complexes and the Balance of T Cell Activation Versus Death. *J. Immunol.* **2001**, *166*, 7229–7237.
47. Harding, C. V.; Unanue, E. R. Antigen Processing and Intracellular Ia. Possible Roles of Endocytosis and Protein Synthesis in Ia Function. *J. Immunol.* **1989**, *142*, 12–19.
48. Bishop, G. A.; Waugh, J. A.; Hall, B. M. Expression of Hla Antigens on Renal Tubular Cells in Culture: II. Effect of Increased Hla Antigen Expression on Tubular Cell Stimulation of Lymphocyte Activation and on Their Vulnerability to Cell-Mediated Lysis. *Transplantation* **1988**, *46*, 303–310.
49. Nietosvaara, Y.; Renkonen, R.; Mattila, P.; Hyry, P. Cultured Rat Kidney Parenchymal Components Are Damaged by Cytotoxic Lymphocytes Produced in Mlc. *APMIS* **1990**, *98*, 724–728.